


## Time-Delay Model of Nonlinear Frequency Down-Conversion in the Cavity of a Semiconductor Disk Laser

Yu. A. Morozov,<sup>1,\*</sup> M. Yu. Morozov,<sup>1</sup> M.I. Balakin,<sup>2</sup> L.A. Kochkurov,<sup>2</sup> and A.I. Konyukhov<sup>3</sup>

<sup>1</sup>*Kotel'nikov Institute of Radio Engineering and Electronics (Saratov Branch), Russian Academy of Sciences, 38 Zelenaya Street, Saratov 410019, Russia*

<sup>2</sup>*Yuri Gagarin State Technical University of Saratov, 77 Politechnicheskaya Street, Saratov 410054, Russia*

<sup>3</sup>*Saratov State University, 83 Astrakhanskaya Street, Saratov 410012, Russia*

 (Received 9 October 2018; revised manuscript received 29 January 2019; published 10 April 2019)

A model of nonlinear optical interaction in the external cavity of a semiconductor disk laser is derived and numerically studied. The model is formalized in a system of differential equations with time delay (TD). The steady-state operation point, its stability, and transient dynamics of intracavity singly resonant optical parametric oscillators (ICSROs) are analyzed in the framework of this model. Also, the same quantities are studied with the help of the normal-mode expansion (NME) method. Both models result in the same steady-state solution, while the stability and dynamic behavior appear to be quite different. The characteristic equation defining the steady-state stability of the TD dynamic system is shown to have an infinite number of roots that may be grouped into two sets of complex-conjugate pairs. For the TD model, the Hopf bifurcation occurs when the primary pump exceeds the bifurcation value. The characteristic equation corresponding to the NME model in the single-mode approximation has only three roots with the real parts not exceeding zero; i.e., the steady-state operation point maintains stability for all values of the primary pump used in the simulation.

DOI: [10.1103/PhysRevApplied.11.044027](https://doi.org/10.1103/PhysRevApplied.11.044027)

### I. INTRODUCTION

High-resolution spectroscopy is known to need continuous-wave (CW) sources of coherent radiation in the mid- and far-infrared spectral windows. Studying operating characteristics of difference-frequency generators and optical parametric oscillators that are eminently suitable for such an application is thus of great importance [1]. Some realizations of the devices can likely be made simple, compact, and easy to use [2,3]. The compactness of the oscillators may be achieved through using an intracavity setup, i.e., with a nonlinear crystal for parametric interaction located in a short-length cavity. Promising features of the intracavity singly resonant optical parametric oscillator (ICSRO) have been shown by Stothard *et al.* in Ref. [4], where a device pumped by a semiconductor disk laser (SDL) was demonstrated. Unfortunately, their ICSRO does not allow pump and signal wavelengths to be very close to each other (i.e., to emit longer wavelength idler radiation). In our approach [2], by using a single cavity shared by the pump and signal emission, this shortcoming may be fixed. Moreover, as it has been theoretically proposed in Ref. [3], both the intracavity difference-frequency generator

(ICDFG) and the ICSRO can potentially be built according to the approach.

One of the factors that determine the suitability of these devices for these applications is the stability of steady-state radiation. To examine that, one should use the equations of motion that formalize the dynamic behavior of the oscillators. Most mathematical models of intracavity oscillators based on nonlinear optical frequency conversion apply the expansion of resonating fields in a set of normal modes of the cavities [3,5–10] [the so-called Slater normal-mode expansion (NME) [11]].

This approach usually implies averaging small spatial field variations over the length of corresponding cavities [8,9]. If one mode is examined (or multimode fields with nonsynchronous components are analyzed), such an approach results in slow variations of the field amplitudes on the scale of a cavity round-trip time. On the other hand, the electrostatics itself does not prohibit faster amplitude oscillations. The only condition that has to be fulfilled is the small amplitude variations (or the absence of such variations under continuous-wave operation) for the time moments taken every multiple of the round-trip time in a device with a high-finesse cavity.

To study the possibility of such fast amplitude oscillations (which may appear to be the origin of instability of a steady-state operation regime), we use the model of a

\*yuri.mor@rambler.ru

laser with coupled cavities [12–15]. One of the cavities, named a subcavity, is formed between a semiconductor distributed double-band Bragg mirror (DBM) grown inside a laser chip and the emitting surface of the chip. The main (external) laser cavity is terminated by an outer mirror of high reflectivity. It was shown that such a laser, which may be thought of as a dynamic system with a time-delay (TD) feedback of a large value, demonstrates rather complex behavior for appropriate values of laser parameters [15]. The model of a laser is in sharp contrast to the well-known Lang-Kobayashi model [16] that adopts only small reflections from a distant mirror.

The time-delay model of a dual-wavelength SDL was derived in Ref. [15]. We believe the dynamics of the compact ICSRO and ICDFG [2,3] can be studied in the framework of the TD model of Ref. [15] developed by taking into account the impact of three-wave nonlinear interaction. To be more specific, we have selected the derivation of such a model and its application to the analysis of dynamic behavior of the ICSRO as the main objectives of the manuscript.

## II. DERIVATION OF THE EQUATIONS

### A. Time-delay rate equations

Schematically, the ICSRO is arranged in compliance with Fig. 1. It has a three-mirror design. An external linear cavity closed by a concave mirror of high reflectivity is coupled with a subcavity formed by two mirrors: a DBM and a facet facing the external cavity. The subcavity may also be referred to as the gain mirror. The external cavity is resonant for both the pump at the wavelength of  $1.98 \mu\text{m}$  and the signal at  $2.25 \mu\text{m}$ . Three-wave nonlinear parametric interaction is assumed to be realized in an orientation-patterned quasi-phase-matched (QPM) crystal of GaAs located in the cavity. The idler emission at the wavelength of  $16.5 \mu\text{m}$  does not resonate in the cavity. To ensure high reflectivity of the gain mirror for both the pump and signal fields, we use a DBM [17]. The primary

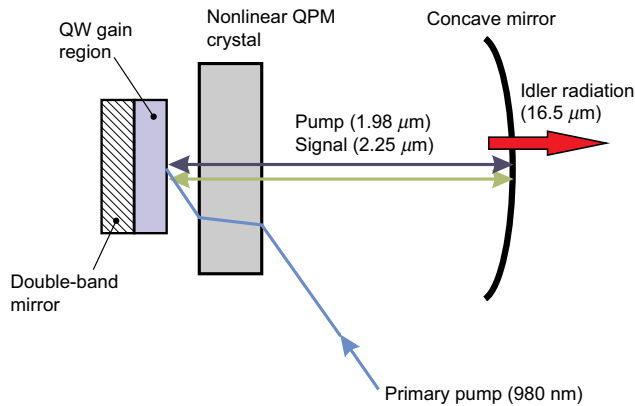


FIG. 1. Schematic setup of the device.

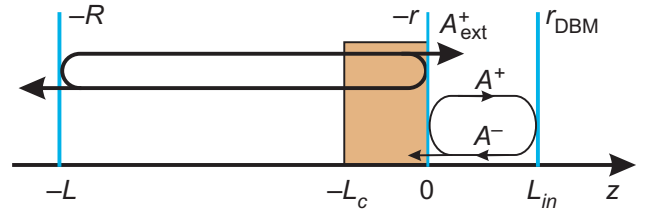


FIG. 2. Schematic diagram of reflections.

pumping at the wavelength of  $980 \text{ nm}$  is implemented by the beam passing through the transparent GaAs nonlinear crystal towards the gain mirror.

The design of the gain mirror does not differ substantially from that of an ordinary SDL: it contains quantum wells (made of  $\text{Ga}_{0.74}\text{In}_{0.26}\text{Sb}$ ) located at the antinode positions of the pump emission in order to provide the maximal use of the available gain (see Ref. [3] for more detail on the design). The schematic diagram of reflections in the lasers under study is shown in Fig. 2. According to the approach of Refs. [12–15], the equations of the mathematical model are formulated for the variables relating to the subcavity (the area of length  $L_{\text{in}}$  in the figure). The impact of optical fields returned from a distant mirror with reflectivity  $-R$  is taken into account by the complex field amplitude  $A_{\text{ext}}^{\pm}$  (signs  $+/-$  correspond to the waves running along the positive/negative directions of axis  $z$  and “ext” abbreviates external). Let

$$r_{\text{ef}} = \frac{A^+(+0, t) + A_{\text{ext}}^+(+0, t)}{A^-(-0, t)} \quad (1)$$

be the effective reflectivity of the inner facet viewed from inside the subcavity. From now on, the symbol  $+0$  defining the spatial position is not written, i.e.,  $A^{+,-}(+0, t) = A^{+,-}(t)$ . Here, complex amplitudes  $A^{+,-}$  represent the optical fields in the subcavity without contribution of reflections from the external cavity. Then, by accounting for multiple reflections from the distant mirror, one can derive [15]

$$r_{\text{ef}} = r \left[ 1 - \chi \sum_{m=1}^{\infty} (R_{\text{ef}} r)^{m-1} \frac{A^+(t - m\tau)}{A^+(t)} e^{-j\omega m\tau} \right]. \quad (2)$$

Here,  $\chi = R_{\text{ef}}(1 - r^2)/r$ ,  $\omega$  is the angular frequency of a correspondent electric field, and  $\tau$  is the round-trip time in the external cavity. Since  $r \ll 1$  for the antireflection coated facet, one can take into consideration only a single round-trip in the equation to have

$$r_{\text{ef}} = r \left( 1 - \chi \frac{A_{\tau}^+}{A^+} e^{-j\omega\tau} \right). \quad (3)$$

To shorten equations, we write the subscript  $\tau$  for the quantities taken at the time  $t - \tau$ . In contrast to Ref. [15], the

effective time-dependent nonlinear reflectivity of the outer mirror is introduced as

$$R_{\text{efl}} = R [1 - \mu(f_2 + f_{2\tau})]^{1/2} \quad (4)$$

for the pump emission and as

$$R_{\text{ef2}} = R [1 + \mu(f_1 + f_{1\tau})]^{1/2} \quad (5)$$

for the signal. Here,  $f_i$  corresponds to the one-sided photon flow of the pump ( $i = 1$ ) and the signal radiation ( $i = 2$ ). These fields are supposed to be Gaussian beams with the waist radii  $w_1$  and  $w_2$ ,  $\mu = 2\gamma/[\pi(w_1^2 + w_2^2)]$ ,

$$\gamma = \frac{32Z_0}{n_1 n_2 n_3} d_{14}^2 \left( \frac{L_c^2}{\lambda_1 \lambda_2} \right) \hbar \omega_3, \quad (6)$$

$Z_0 = 120\pi$  is the impedance of free space,  $d_{14}$  is the element of the nonlinear susceptibility tensor of GaAs crystal,  $L_c$  is the length of the crystal,  $\lambda_1$  and  $\lambda_2$  are the wavelengths of the pump and signal,  $n_{1,2,3}$  are the refractive indices, and  $\hbar \omega_3$  is the photon energy of the idler emission.

Equation (3) in combination with Eqs. (4) and (5) appears to be sufficient to derive the rate equations written in terms of the pump and signal total photon numbers in the subcavity (see the Appendix for more details). After the addition of the appropriate equation for the carrier number in the active region of the gain mirror, the following system of the rate equations can be obtained:

$$\begin{aligned} \dot{a}_1 &= \eta \left[ (G_1 - 1) + \frac{1}{T} \left( \frac{a_{1\tau}}{a_1} - 1 \right) - \frac{\delta}{T} (a_2 + a_{2\tau}) \right] a_1, \\ \dot{a}_2 &= \eta \left[ -1 + \frac{1}{T} \left( \frac{a_{2\tau}}{a_2} - 1 \right) + \frac{\delta}{T} (a_1 + a_{1\tau}) \right] a_2, \\ \dot{\nu}_1 &= \sigma - \nu_1 - G_1 a_1. \end{aligned} \quad (7)$$

Here, the photon numbers  $a_i$  and carrier numbers  $\nu_1$  are normalized to  $a_{10}$  and  $\nu_{1\text{th}}$ , respectively.  $a_{10} = \nu_{1\text{th}}/\eta$ , where  $\eta = \tau_r/\tau_{\text{ph}}$ ,  $\tau_r$  and  $\tau_{\text{ph}} = (v_g \alpha_s)^{-1}$  are the lifetimes of carriers and photons in the subcavity,  $\nu_{1\text{th}}$  is the threshold value of the carrier number, and  $T = 2\alpha_s L_{\text{in}} \ll 1$  is the round-trip loss. The normalized gain factor  $G_1$  is simulated in accordance with [3,18,19]

$$G_1 = 1 + G_{10} \ln \nu_1, \quad (8)$$

where  $G_{10} = 4mG_{\text{QW}}/T$ ,  $m$  is the number of quantum wells (QWs) in the active region, and  $G_{\text{QW}}$  is the gain factor

per QW. Having these parameters in mind, the threshold value of the carrier number may be defined as  $\nu_{1\text{th}} = m\pi w_{\text{pp}}^2 N_i \exp(1/G_{10})$ , where  $w_{\text{pp}}$  is the primary pump beam radius and  $N_i$  is the transparent carrier density. The factor of nonlinear interaction is denoted as  $\delta = \mu a_{10}/\tau_{\text{in}}$ , where  $\tau_{\text{in}} = 2L_{\text{in}}/v_g$  is the round-trip time in the subcavity. The primary pump  $P$  normalized to the threshold value  $P_{\text{th}}$  is denoted by  $\sigma$ . When deriving Eq. (7), we introduce the normalized time  $t/\tau_r$ . The dots above the variables mean the differentiation over this quantity.

## B. Normal-mode expansion method

It is of interest to compare the simulation results obtained in the framework of two models: (i) the TD model, implying that the dynamic variables are examined in a part of the device (more specifically, in the subcavity), and the impact of a remainder is taken into account in the form of reflections delayed by a multiple round-trip time [Eq. (7)] and (ii) the NME model, where the running field amplitudes are averaged over the cavity length [8,9,11]. The last model has been applied in Ref. [10] to analyze the multimode behavior of the ICSRO.

By using the similar normalization as that used in Eq. (7) and taking into account the single-mode optical fields, one can modify Eq. (9) from Ref. [10] to derive the following rate equations:

$$\begin{aligned} \dot{b}_1 &= \Theta \left[ (G_1 - 1) - \frac{2\delta}{T} b_2 \right] b_1, \\ \dot{b}_2 &= \Theta \left[ -1 + \frac{2\delta}{T} b_1 \right] b_2, \\ \dot{\nu}_1 &= \sigma - \nu_1 - G_1 b_1. \end{aligned} \quad (9)$$

Here, the photon numbers  $b_{1,2}$  that correspond to the laser cavity of length  $L$  are normalized to  $b_{10} = \nu_{1\text{th}}/\Theta$ , where  $\Theta = \tau_r/\tau_{\text{ph}}$  and  $\tau_{\text{ph}}$  is the photon lifetime in the laser cavity. It is easily seen that systems of Eqs. (7) and (9) resemble each other. Moreover, they appear to have the same steady-state solutions:

$$\begin{aligned} a_1 &= b_1 = \frac{T}{2\delta}, \\ a_2 &= b_2 = \frac{T}{2\delta} (G_1 - 1), \\ \sigma - \nu_1 - G_1 \frac{T}{2\delta} &= 0. \end{aligned} \quad (10)$$

However, the transient behavior of the dynamic systems represented by Eqs. (7) and (9) is quite different. Indeed, the NME model in Eq. (9) results in slow amplitude

variations on the scale of the round-trip time  $\tau$ ,

$$\dot{b}_{1,2} \sim -\Theta b_{1,2},$$

or when differentiating over the usual time,

$$\frac{db_{1,2}}{dt} \sim -\frac{\Theta}{\tau_r} b_{1,2} = -\frac{b_{1,2}}{\tau_{\text{PH}}} \ll -\frac{b_{1,2}}{\tau}.$$

Faster amplitude variations may be studied with the help of the TD model only, as shown further [see Figs. 5(a) and 6 below].

From Eq. (9) with  $b_2 = a_2 = 0$ , one can obtain the value of the pump parameter  $\sigma$  at the threshold of parametric generation  $\sigma_{\text{OPO}} = 1 + T/(2\delta)$ .

### III. NUMERICAL RESULTS

#### A. Steady-state stability

First, let us compare the linear stability of steady-state operation of the dynamical systems represented by Eqs. (7) and (9). The TD differential equations in Eq. (7) can be analyzed with the help of the DDEBIFTOOL package [20], while the NME model represented by Eq. (9) can be studied with the standard approach (see, e.g., Ref. [21]).

The characteristic equation corresponding to the steady-state point of Eq. (7) has an infinite number of roots  $\Lambda$  that can be combined into four sets as follows:

$$\begin{aligned} \Lambda_n^{(1,3)} &= \text{Re}(\Lambda_n^{(1)}) \pm j \text{Im}(\Lambda_n^{(1)}), \\ \Lambda_n^{(2,4)} &= \text{Re}(\Lambda_n^{(2)}) \pm j \text{Im}(\Lambda_n^{(2)}). \end{aligned} \quad (11)$$

Here, the superscripts stand for the set's number, while the subscript  $n = 1, \dots, \infty$  gives the number of the root. [There are a few real roots as well with negative values of much less than those of Eq. (11), which do not contribute considerably to the stability of the steady state.] One can see that sets 1 and 2 are located in the upper half of the plane of complex numbers; sets 3 and 4 can be obtained via the mirror reflection of sets 1 and 2 into the lower half-plane. For distinctness, let us assume set 1 to contain the roots with maximal values of real parts. These roots mainly determine the stability of the steady-state operation. The imaginary parts of the roots appear to be approximately equal to the multiples of the intermode beat frequency:

$$\text{Im}(\Lambda_n^{(1,2)}) \approx 2\pi n/\tau. \quad (12)$$

All of these findings, including the grouping of roots into four sets represented by Eq. (11) and the specific separation of the imaginary parts of the roots in Eq. (12), agree with those of the theory of dynamic systems with large delay [22].

Figure 3 displays the roots of the characteristic equation of the TD dynamic system in Eq. (7) (sets 1 and 2 are

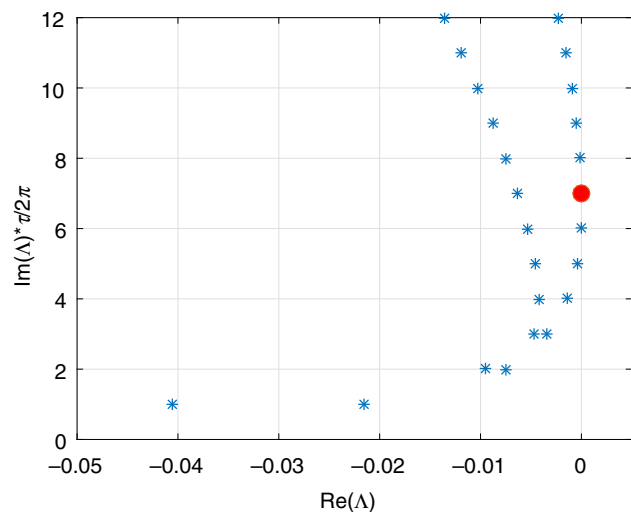


FIG. 3. Characteristic equation's roots with positive imaginary parts.

only shown). The simulations are performed with the following parameters:  $L = 30$  mm,  $L_c = 5$  mm,  $L_{\text{in}} = 5$   $\mu\text{m}$ ,  $\lambda_1 = 1.98$   $\mu\text{m}$ ,  $\lambda_2 = 2.25$   $\mu\text{m}$ ,  $w_1 = w_2 = 80$   $\mu\text{m}$ ,  $w_{\text{PP}} = 90$   $\mu\text{m}$ ,  $d_{14} = 1.0 \times 10^{-4}$   $\mu\text{m/V}$ ,  $n_1 \approx n_2 = 3.335$ ,  $n_3 = 3.22$ ,  $T = 0.025$ ,  $\tau_r = 2 \times 10^{-9}$  s,  $N_l = 1.45 \times 10^{12}$   $\text{cm}^{-2}$ , and  $G_{\text{QW}} = 2.5 \times 10^{-3}$  [19]. We take that the active region of the ICSRO includes  $m = 10$  QWs. The primary pump light for the SDL is assumed to be supplied by a diode laser at 980 nm. When simulating the graphs presented in Fig. 3, we choose the value of primary pump parameter  $\sigma = 2.257\sigma_{\text{OPO}} = 24.9$ . With given values of the parameters, the dynamic system in Eq. (7) is near the boundary of steady-state stability: there is the pair of complex-conjugate roots with the real part approaching zero (one of the roots is marked by the red circle in the figure). One can thus conclude that the steady-state stability is violated via the Hopf bifurcation.

As for the NME model of the same ICSRO in Eq. (9), the corresponding characteristic equation has three roots with negative real parts; i.e., the steady-state solution appears to be stable under all allowable values of the parameters.

To study the stability of the steady-state operation in more detail, we simulate the behavior of a few roots of the characteristic equation as functions of the primary pump parameter  $\sigma$ . Figure 4(a) shows the dependence of the real parts of the roots belonging to set 1 on the normalized pump of the ICSRO. The symbols 6, ..., 9 near the curves correspond to the indices  $n$  of the roots. One can see that the branch consisting of  $\text{Re}(\Lambda_7^{(1)})$  has the minimal bifurcation value  $\Sigma_H = \sigma/\sigma_{\text{OPO}} = 2.257$  (compare with Fig. 3) and the device keeps stability within  $1 \leq \sigma/\sigma_{\text{OPO}} \leq \Sigma_H$ .

In Fig. 4(b), we plot the real part of the root of the characteristic equation corresponding to the NME model in Eq. (9) vs the pump of the device (the root with the maximal

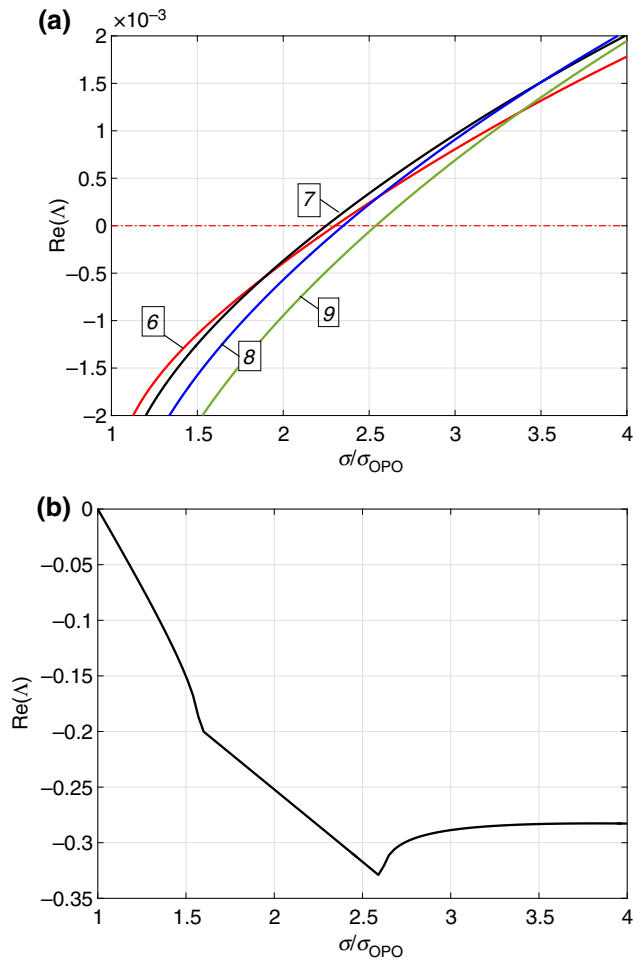


FIG. 4. Real parts of the characteristic equation versus  $\sigma/\sigma_{\text{OPO}}$  in the model of the TD system (a) and the NME model (b). The numbers near the curves in (a) correspond to the roots' numbers.

real part is shown). The breaks of the curve correspond to the change of the root from the purely real one to the complex-conjugate pair. It is easily seen that this model predicts the steady-state stability along the whole taken interval of the normalized primary pump parameter.

### B. Transient dynamics of the ICSRO

The analysis of the steady-state stability is confirmed by the simulations of the transient dynamics performed according to Eqs. (7) and (9). Figure 5(a) shows the dynamics of the ICSRO formalized in the framework of the TD model, while Fig. 5(b) refers to the simulations of the NME model. The normalized primary pump parameter  $\sigma/\sigma_{\text{OPO}} = 1.81$  is taken to be below the bifurcation value  $\Sigma_H$  of the TD model; i.e., the steady-state solution is expected to be stable. Indeed, from Fig. 5(a), one can see that, after the relaxation oscillations that are clearly visible in the time interval  $10 \leq t/\tau_r \leq 2 \times 10^3$ , both the pump (1) and signal (2) emissions eventually come to the

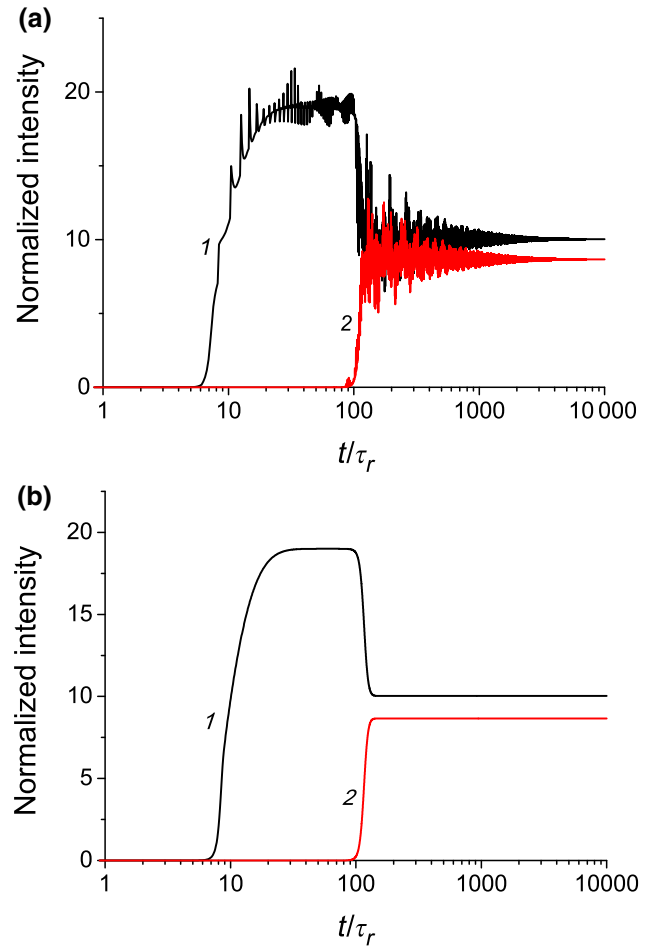


FIG. 5. Transient dynamics simulated according to the model of the TD system (a) and to the NME model (b). The pump (1) and signal (2) emissions are shown.

steady-state operation point. The duration of the relaxation oscillations agrees well with the one evaluated from decrement  $\text{Re}(\Lambda)$  given in Fig. 4(a).

As should be expected from the data of Fig. 4(b), deviations from the steady-state point die out very fast [they need just a few  $\tau_r$ 's to be suppressed and cannot thus be visible in the scale of Fig. 5(b)]. From Figs. 5(a) and 5(b), one can easily see as well that the pump emission needs about  $10\text{--}20 \tau_r$ 's to develop and to serve as an origin of the signal stimulated emission in approximately  $100 \tau_r$ .

It is of interest to trace the dynamics of the TD system beyond the bifurcation value of the stable steady-state operation, i.e., for  $\sigma/\sigma_{\text{OPO}} > \Sigma_H$ . Such dynamics of the pump emission is shown in Fig. 6 for the primary pump parameter  $\sigma/\sigma_{\text{OPO}} = 3.62$ . The instability of the steady-state operation needs the order of  $10^3 \tau_r$  to be developed. After that, the emission exists in the form of complicated oscillations that are nearly periodic on the small scale of the round-trip time  $\tau$ ; the amplitude of the oscillations slowly varies (on the scale of about  $10^3 \div 10^4$  of such

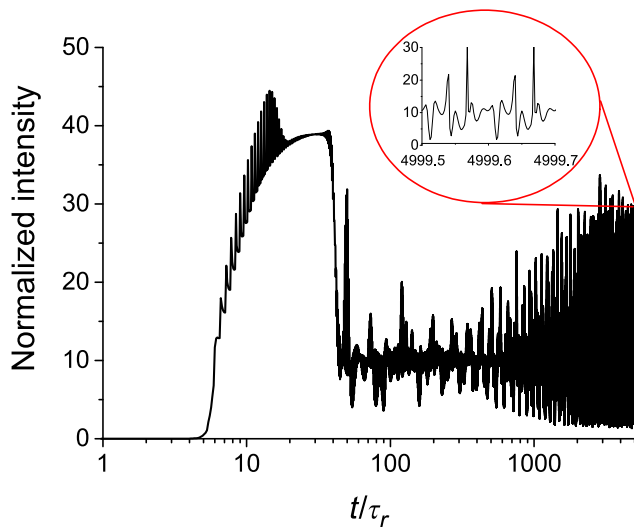


FIG. 6. Pump emission dynamics for  $\sigma/\sigma_{\text{OPO}} > \Sigma_H$ . The trailing part of the graph is shown in the inset.

a time interval). Two “periods” of the oscillations corresponding to the trailing part of the dynamics are shown in the inset of Fig. 6. The signal emission (not shown here) demonstrates similar dynamics in the operation regime of lost steady-state stability.

It should be noted that the relaxation oscillations resembling those displayed in Fig. 5(a) were observed in a semiconductor laser with strong optical feedback from a distant reflector [23–25]. Indeed, these authors discovered that the intensity oscillations of a semiconductor laser with coupled cavities appear to be resonant with the multiples of the intermode beat frequency of the external cavity.

#### IV. CONCLUSION

We derive and numerically study the TD model of nonlinear optical interaction realized in a cavity of a semiconductor disk laser. This nonlinear interaction results in parametric oscillations accompanied by frequency down-conversion to the mid-infrared band of the electromagnetic spectra. Based on the approach of Refs. [12], [13], [14], and [15], the model is modified to take into account this nonlinear optical interaction.

The steady-state operation point of the ICSRO, its stability, and the dynamics are studied according to this model represented by Eq. (7). The study is supplemented with the analysis of identical characteristics obtained in the framework of the NME model of Eq. (9). Despite the fact that steady-state solutions of both systems in Eqs. (7) and (9) are the same, the stability and dynamics show rather different behaviors for these models. The solution of the characteristic equation that determines the linear stability of the TD system in Eq. (7) has an infinite number of roots grouped mainly into complex-conjugate pairs. The imaginary parts of the roots describe the oscillation frequencies

of small deviations from the steady-state point; their values closely correspond to the multiples of the intermode beat frequency. According to the TD model, the steady-state solution is shown to lose the stability via the Hopf bifurcation that occurs for the value  $\Sigma_H$  of the normalized primary pump.

As for the NME model, the ICSRO keeps the steady-state stability for all values of the primary pump parameter taken in the simulation.

For the primary pump value  $\sigma/\sigma_{\text{OPO}} < \Sigma_H$ , the transient dynamics of the ICSRO simulated with the TD model displays the long-lived (approximately  $10^3 \tau_r$ ) oscillations of the pump and signal intensities, relaxing eventually to the steady-state operation point. This transition time (about a few microseconds) is still much less than the mean time between adjacent moments of parameter disturbances that originated from technical noise. The output radiation of the ICSRO may thus be assumed to be a dynamically single mode and suitable for spectroscopy applications.

The NME model demonstrates much faster collapsing to the steady state without noticeable traces of oscillations.

Above the bifurcation value  $\Sigma_H$ , the instability of the steady-state operation develops and the emission finally emerges in the form of multiscaled oscillations of high intensity. Being examined on the small scale, the time period of the oscillations is nearly equal to the round-trip time of the cavity. An oscillation amplitude varies on the scale of  $10^3 \div 10^4$  of  $\tau$ .

#### ACKNOWLEDGMENT

This study was funded by RFBR according to the research project Grant No. 18-08-00599-a.

#### APPENDIX

Let us begin with the Manly-Rowe relations for parametric nonlinear interaction [26]:

$$\begin{aligned} \frac{\partial(f_1 + f_3)}{\partial z} &= 0, \\ \frac{\partial(f_2 - f_3)}{\partial z} &= 0. \end{aligned} \quad (\text{A1})$$

These equations may be written as

$$\begin{aligned} f_1|_{\text{in}} + f_3|_{\text{in}} &= f_1|_{\text{out}} + f_3|_{\text{out}}, \\ f_2|_{\text{in}} - f_3|_{\text{in}} &= f_2|_{\text{out}} - f_3|_{\text{out}}, \end{aligned} \quad (\text{A2})$$

where  $|_{\text{in/out}}$  corresponds to the input/output cross section of the nonlinear crystal. The dependence on time is not written. Since there is no cavity for the idler emission, one

can assume  $f_3|_{\text{in}} = 0$ . Bearing in mind that

$$f_3|_{\text{out}} = \mu(f_1 f_2)|_{\text{in}}, \quad (\text{A3})$$

(see, e.g., Ref. [27]), the following equations can be obtained:

$$\begin{aligned} f_1|_{\text{out}} &= f_1|_{\text{in}} (1 - \mu f_2|_{\text{in}}), \\ f_2|_{\text{out}} &= f_2|_{\text{in}} (1 + \mu f_1|_{\text{in}}). \end{aligned} \quad (\text{A4})$$

These relations represent the photon flow transformation when passing through the nonlinear crystal (the nonlinear interaction is supposed to be lumped; i.e., a time delay in the crystal is disregarded). Equation (A3) holds, assuming the length  $L_c$  to be much less than the Rayleigh length for the pump and signal beams.

As the nonlinear crystal is located in the immediate vicinity of the subcavity, the field passages through the nonlinear crystal are separated by  $\tau$  in time. That is why we come to Eqs. (4) and (5) of the manuscript [with the additional assumption  $\mu(f + f_\tau) \ll 1$  taken into account].

According to Ref. [15], one can derive the rate equation describing the pump photon density:

$$\frac{dS_1}{dt} = v_g \left[ \Gamma_1 g_1 - \alpha_{\text{in}} + \frac{1}{L_{\text{in}}} \ln(r_{\text{DBM}}|r_{\text{ef}}|) \right] S_1. \quad (\text{A5})$$

Here,  $\Gamma_1$  and  $g_1$  are the confinement factor and the gain coefficient for the pump emission,  $\alpha_{\text{in}}$  is the loss factor because of scattering and nonresonant absorption in the subcavity, and  $v_g$  is the group velocity. With  $\chi \gg 1$ , we have from Eq. (3)

$$|r_{\text{ef}}| \approx R_{\text{ef}}(1 - r^2) \frac{|A_\tau^+|}{|A^+|}. \quad (\text{A6})$$

By substituting Eq. (A6) into Eq. (A5), we arrive at

$$\begin{aligned} \frac{dS_1}{dt} &= v_g \left\{ \Gamma_1 g_1 - \alpha_s \right. \\ &\quad \left. + \frac{1}{2L_{\text{in}}} \left[ \left( \frac{S_{1\tau}}{S_1} - 1 \right) - \mu v_g \frac{\pi w_2^2}{4} (S_2 + S_{2\tau}) \right] \right\} S_1, \end{aligned} \quad (\text{A7})$$

where  $\alpha_s = \alpha_{\text{in}} - (L_{\text{in}})^{-1} \ln[r_{\text{DBM}}(1 - r^2)R]$ . Equation (4) and the expression  $f = S v_g \pi w^2/4$  relating the flow  $f$  and the photon density  $S$ , as well as the assumption that  $|A_\tau^+|/|A^+| \approx [S_\tau/S]^{1/2} \approx 1$ , are used here.

In our opinion, the rate equations written in terms of the total photon numbers are more convenient for the analysis and simulation than those in terms of the photon densities.

Keeping in mind that the total photon numbers  $a_i a_{i0}$  in the  $i$ th optical field may be represented as

$$a_i a_{i0} = S_i \frac{\pi w_i^2}{2} L_{\text{in}}, \quad (\text{A8})$$

one can derive the first equation from the system of equations in Eq. (7):

$$\dot{a}_1 = \eta \left[ (G_1 - 1) + \frac{1}{T} \left( \frac{a_{1\tau}}{a_1} - 1 \right) - \frac{\delta}{T} (a_2 + a_{2\tau}) \right] a_1.$$

Here,  $G_1 = \Gamma_1 g_1 v_g \tau_{\text{ph}} = G_{10} \ln [v_1 v_{1\text{th}} / (m \pi w_{\text{pp}}^2 N_t)] = 1 + G_{10} \ln v_1$  [see Eq. (8) and Refs. [3, 18, 19] for more details]. The second equation of Eq. (7) is obtained in a similar way by assuming the signal field gain factor  $G_2 = 0$ . The equation for the carrier number in the active region of the gain mirror does not significantly differ from that of an ordinary semiconductor disk laser (e.g., Ref. [28]).

- 
- [1] I. T. Sorokina and K. L. Vodopyanov, eds. *Solid-State Mid-Infrared Laser Sources* (Springer-Verlag, Berlin Heidelberg, 2003), p. 558.
  - [2] Yu. A. Morozov, M. Yu. Morozov, V. I. Kozlovsky, and O. G. Okhotnikov, Compact intracavity singly-resonant optical parametric oscillator pumped by GaSb-based vertical external cavity surface-emitting laser: Concept and the main operational characteristics, *IEEE J. Select. Top. Quantum Electron.* **21**, 1603105 (2015).
  - [3] Yu. A. Morozov, Multi-mode dynamics of optical oscillators based on intracavity nonlinear frequency down-conversion, *Appl. Phys. B* **124**, 12 (2018).
  - [4] D. J. M. Stothard, J.-M. Hopkins, D. Burns, and M. H. Dunn, Stable continuous-wave, intracavity, optical parametric oscillator pumped by a semiconductor disk laser (VECSEL), *Opt. Express* **17**, 10648 (2009).
  - [5] M. K. Oshman and S. E. Harris, Theory of optical parametric oscillation internal to the laser cavity, *IEEE J. Quantum Electron.* **QE-4**, 491 (1968).
  - [6] J. Falk, J. M. Yarborough, and E. O. Ammann, Internal optical parametric oscillation, *IEEE J. Quantum Electron.* **QE-7**, 359 (1971).
  - [7] S. E. Hodges, M. Munroe, J. Cooper, and M. G. Raymer, Multimode laser model with coupled cavities and quantum noise, *JOSA B* **14**, 191 (1997).
  - [8] T. Debuisschert, J. Raffy, J. P. Pocholle, and M. Papuchon, Intracavity optical parametric oscillator: Study of the dynamics in pulsed regime, *JOSA B* **13**, 1569 (1996).
  - [9] G. A. Turnbull, M. H. Dunn, and M. Ebrahimzadeh, Continuous-wave, intracavity optical parametric oscillators: An analysis of power characteristics, *Appl. Phys. B* **66**, 701 (1998).
  - [10] Yu. A. Morozov, Transient power characteristics of a compact singly resonant intracavity optical parametric oscillator pumped by a semiconductor disk laser, *JOSA B* **33**, 1470 (2016).

- [11] A. E. Siegman, *Lasers* (University Science Book, Mill Valley, California, 1986), p.1304.
- [12] J.-D. Park, D.-S. Seo, and J. McInerney, Self-pulsations in strongly coupled asymmetric external cavity semiconductor lasers, *IEEE J. Quantum Electron.* **26**, 1353 (1990).
- [13] R.-Q. Hui and S.-P. Tao, Improved rate equations for external cavity semiconductor lasers, *IEEE J. Quantum Electron.* **25**, 1580 (1989).
- [14] G. H. M. van Tartwijk and D. Lenstra, Semiconductor laser with optical injection and feedback, *Quantum Semiclass Opt.* **7**, 87 (1995).
- [15] A. Morozov, T. Leinonen, A. Härkönen, and M. Pessa, Simultaneous dual-wavelength emission from vertical external-cavity surface-emitting laser: A numerical modeling, *IEEE J. Quantum Electron.* **42**, 1055 (2006).
- [16] R. Lang and K. Kobayashi, External optical feedback effects on semiconductor injection laser properties, *IEEE J. Quantum Electron.* **16**, 347 (1980).
- [17] S. Calvez, D. Burns, and M. D. Dawson, Optimization of an optically pumped 1.3- $\mu\text{m}$  GaInNAs vertical-cavity surface-emitting laser, *IEEE Photon. Techn. Lett.* **14**, 131 (2002).
- [18] P. S. Zory, ed. *Quantum-well lasers* (Acad. Press, San Diego, 1993), p. 504.
- [19] M. Rattunde, J. Schmitz, C. Mermelstein, R. Kiefer, and J. Wagner, in *Mid-Infrared Semiconductor Optoelectronics*, Springer Series in Optical Sciences, edited by A. Krier (Springer-Verlag London Limited, 2006) p. 131.
- [20] K. Engelborghs, T. Luzyanina, and G. Samaey, *DDE-BIFTOOL v.2.00 user manual: A Matlab package for bifurcation analysis of delay differential equations*, Tech. Rep. TW 330 (Katholieke Universiteit Leuven, Leuven, Belgium, 2001).
- [21] D. W. Jordan and P. Smith, *Nonlinear ordinary differential equations. An introduction for scientists and engineers*, (Oxford, New York, 2007), 4th ed., p. 531.
- [22] S. Yanchuk and G. Giacomelli, Spatio-temporal phenomena in complex systems with time delays, *J. Phys. A: Math. Theor.* **50**, 103001 (56pp) (2017).
- [23] J. P. Toomey, D. M. Kane, M. W. Lee, and K. A. Shore, Nonlinear dynamics of semiconductor lasers with feedback and modulation, *Opt. Express* **18**, 16955 (2010).
- [24] B. Kelleher, M. J. Wishon, A. Locquet, D. Goulding, B. Tykalewicz, G. Huyet, and E. A. Viktorov, Delay induced high order locking effects in semiconductor lasers, *Chaos* **27**, 114325-1 (2017).
- [25] B. Tykalewicz, D. Goulding, S. P. Hegarty, G. Huyet, T. Erneux, B. Kelleher, and E. A. Viktorov, Emergence of resonant mode-locking via delayed feedback in quantum dot semiconductor lasers, *Opt. Express* **24**, 4239 (2016).
- [26] X. Liu, H. Zhang, and M. Zhang, Exact analytical solutions and their applications for interacting waves in quadratic nonlinear medium, *Opt. Express* **10**, 83 (2002).
- [27] D. Richter, A. Fried, and P. Weibring, Difference frequency generation laser based spectrometers, *Laser Photon. Rev.* **3**, 343 (2009).
- [28] A. C. Tropper and S. Hoogland, Extended cavity surface-emitting semiconductor lasers, *Prog. Quantum Electron.* **30**, 1 (2006).